HHS Public Access

Author manuscript

Neuroimage. Author manuscript; available in PMC 2023 April 12.

Published in final edited form as:

Neuroimage. 2022 November 01; 261: 119503. doi:10.1016/j.neuroimage.2022.119503.

Susceptibility networks reveal independent patterns of brain iron abnormalities in multiple sclerosis

Jack A. Reeves[a,d], **Niels Bergsland**[a,d,f], **Michael G. Dwyer**[a,b,d], **Gregory E. Wilding**[c], **Dejan Jakimovski**[a,d], **Fahad Salman**[a,d], **Balint Sule**[a,d], **Nicklas Meineke**[a,d], **Bianca Weinstock-Guttman**[d,e], **Robert Zivadinov**[a,b,d], **Ferdinand Schweser**[a,b,d]

[a.]Buffalo Neuroimaging Analysis Center, Buffalo, NY, USA

[b.]Center for Biomedical Imaging, Clinical and Translational Science Institute, State University of New York at Buffalo, Buffalo, NY, USA

[c.]Department of Biostatistics, School of Public Health and Health Professions, State University of New York at Buffalo, Buffalo, NY, USA

[d.]Department of Neurology, Jacobs School of Medicine and Biomedical Sciences, State University of New York at Buffalo, Buffalo, NY, USA

[e.]Jacobs Neurological Institute, Buffalo, NY, USA

[f.]MR Research Laboratory, IRCCS, Don Gnocchi Foundation ONLUS, Milan, Italy

Abstract

Brain iron homeostasis is necessary for healthy brain function. MRI and histological studies have shown altered brain iron levels in the brains of patients with multiple sclerosis (MS), particularly in the deep gray matter (DGM). Previous studies were able to only partially separate iron-modifying effects because of incomplete knowledge of iron-modifying processes and influencing factors. It is therefore unclear to what extent and at which stages of the disease different processes contribute to brain iron changes. We postulate that spatially covarying magnetic susceptibility networks determined with Independent Component Analysis (ICA) reflect, and allow for the study of, independent processes regulating iron levels.

We applied ICA to quantitative susceptibility maps for 170 individuals aged 9 to 81 years without neurological disease ("Healthy Aging" (HA) cohort), and for a cohort of 120 patients with MS and 120 age- and sex-matched healthy controls (HC; together the "MS/HC" cohort).

Two DGM-associated "susceptibility networks" identified in the HA cohort (the Dorsal Striatum and Globus Pallidus Interna Networks) were highly internally reproducible (i.e. "robust") across multiple ICA repetitions on cohort subsets. DGM areas overlapping both robust networks had higher susceptibility levels than DGM areas overlapping only a single robust network, suggesting that these networks were caused by independent processes of increasing iron concentration. Because MS is thought to accelerate brain aging, we hypothesized that associations between age and the two robust DGM-associated networks would be enhanced in patients with MS. However,

Correspondence to: Ferdinand Schweser, 6045C Clinical and Translational Research Center, 875 Ellicott Street, Buffalo, New York, 14203, schweser@buffalo.edu.

only one of these networks was altered in patients with MS, and it had a null age association in patients with MS rather than a stronger association. Further analysis of the MS/HC cohort revealed three additional disease-related networks (the Pulvinar, Mesencephalon, and Caudate Networks) that were differentially altered between patients with MS and HCs and between MS subtypes. Exploratory regression analyses of the disease-related networks revealed differential associations with disease duration and T2 lesion volume. Finally, analysis of ROI-based disease effects in the MS/HC cohort revealed an effect of disease status only in the putamen ROI and exploratory regression analysis did not show associations between the caudate and pulvinar ROIs and disease duration or T2 lesion volume, showing the ICA-based approach was more sensitive to disease effects.

These results suggest that the ICA network framework increases sensitivity for studying patterns of brain iron change, opening a new avenue for understanding brain iron physiology under normal and disease conditions.

Keywords

Iron; network; QSM; multiple sclerosis; aging

1. Introduction

Maintaining brain iron homeostasis is key in regulating healthy brain function. Iron is required for normal metabolic processes in the brain such as myelination and neurotransmitter synthesis (Connor and Menzies, 1996; Kuhn et al., 1980). However, excess iron that is not properly sequestered (e.g. as cytosolic ferritin) can have deleterious effects through the formation of reactive oxygen species (Dixon and Stockwell, 2014). A variety of factors can alter the iron homeostasis in the brain including healthy aging (Daugherty and Raz, 2013; Hallgren and Sourander, 1958; Li et al., 2021), behavioral factors such as body mass index (BMI) and cigarette smoking (Li et al., 2021), as well as neurological disorders including Parkinson's disease and multiple sclerosis (MS) (Acosta-Cabronero et al., 2017; Stankiewicz et al., 2014).

In MS, increased iron concentrations have been reported in the putamen, caudate, and other deep gray matter (DGM) regions and decreased concentrations have been noted in the thalamus (Khalil et al., 2015; Stankiewicz et al., 2014; Walsh et al., 2013). Increased iron has also been noted in the Rolandic cortex, although at a lower frequency than for DGM iron changes (Bakshi et al., 2000). Iron is also know to concentrate at the rim of chronically active WM lesions within microglia (Gillen et al., 2018) whereas post mortem studies suggested that iron is depleted from normally-appearing WM (Hametner et al., 2013). These iron alterations may be caused by a variety of different cellular or biochemical mechanisms, such as altered iron transport across the blood-brain barrier, inflammatory activity, or iron depletion from glial syncytium (decreased concentration) (Schweser et al., 2018; Stankiewicz et al., 2014).

Brain iron levels can be monitored in vivo by using iron-sensitive MRI techniques such as quantitative susceptibility mapping (QSM), which measures the magnetic susceptibility of

tissues (Reichenbach et al., 2015; Schweser et al., 2016, 2011). QSM signals are thought to reflect paramagnetic iron, which increases the magnetic susceptibility (Langkammer et al., 2012), and diamagnetic myelin, which decreases the susceptibility (Hametner et al., 2018). Therefore, increased susceptibility may arise from either increased iron levels or demyelination, whereas decreased susceptibility may arise from decreased iron levels or increased myelin. The codependence on myelin complicates the interpretation of MRI-based measurements of iron with most techniques, including QSM, particularly under conditions where both myelin and iron may be altered.

Most previous studies analyzed brain images either using region-of-interest (ROI) based approaches, which consider iron dynamics in each deep gray matter region independent from other regions, or voxel-wise approaches, which consider each voxel separately. A limitation of these approaches is that they cannot reveal *overlaying, independent* patterns of iron change; the detected signal change is always the sum of the iron changes of all contributing factors. Separating overlaying effects of iron change is critical for the understanding of the iron physiology of neurological diseases, such as MS, because the patterns may have different relationships to the underlying disease processes and act at different stages of the disease.

We propose using independent component analysis (ICA) to identify the overlapping patterns of iron change in the brain, and postulate that this strategy allows for improved separation of disease-related effects from healthy aging effects as compared to traditional ROI-based analysis. ICA is advantageous because it decomposes a set of signals that were created by mixing (adding) a number of unknown “source” signals into a set of *statistically independent* estimated source signals (“independent components” or “ICs”), which are approximations of the unknown true source signals (Comon, 1994). When applied to QSM, ICA decomposes a set of susceptibility maps, each resulting from a number of overlapping biological processes, into susceptibility networks (or simply “networks” based on standard ICA nomenclature) (McKeown et al., 2003), each of which represents a statistically independent pattern of susceptibility change. ICA has the additional advantages of obtaining outcome measures without prior assumptions on involved anatomical regions in a hypothesis-free manner and without reference to external variables such as subject demographics and disease status. ICA explains each observed susceptibility map as the weighted sum of all networks, with network- and subject-specific loading coefficients used as weights (cf. Fig. 1A and 1B). The relationship between areas involved in a network can be revealed by visual analysis of the ICA components (Fig. 1C).

Loading coefficients indicate the relative contribution of a network to the subject’s (measured) susceptibility map and, hence, can be used as the basis for patient-control comparisons to understand if networks are affected by disease-specific susceptibility patterns. Positive loading coefficients add a positive susceptibility contribution to the measured map when multiplied by a positive network area, whereas negative loading coefficients will give a negative contribution (i.e., negative susceptibility). When considering brain iron, this feature is expected to (i) enable the discovery of networks of anatomical regions that are affected by common patterns of iron change and, thereby, (ii) enable the study of disease-specific patterns with higher sensitivity than conventional methods.

A final consideration when interpreting ICA networks is reproducibility across repeated runs. There are an infinite number of solutions to classical ICA decompositions (Tikhonov et al., 1995), implying that ICA decompositions of the same group with different initial conditions, or separate groups from the same population, may yield different sets of networks. This limitation can be overcome by template-matching procedures that pair ICA networks from different decompositions on the basis of spatial similarity (Garrity et al., 2007). Matching of networks implies that a given network is present in both ICA decompositions and has not been split into sub-networks.

The present study sought to determine if DGM-associated susceptibility networks exist in neurologically normal brains, if these networks are altered in MS, and if other abnormal networks are present in patients with MS.

2. Materials and methods

To answer the first question, we identified DGM susceptibility networks and assessed their associations with other regions in the DGM, WM, cerebellum, and cortex in a cohort of individuals referred to as the “healthy aging” (HA) cohort. We focused the analysis on DGM-associated networks for three reasons: (i) Studies showed that DGM iron is associated with a wide variety of behavioral and clinical factors, such as smoking, body mass index (BMI), and neurological diseases (Daugherty and Raz, 2013; Hallgren and Sourander, 1958; Li et al., 2021; Pirpamer et al., 2016; Stankiewicz et al., 2014), (ii) MRI-based iron assessment is most reliable in the DGM (as compared to cortical and white matter regions) (Schweser et al., 2011), and (iii) most previous QSM studies focused on DGM regions facilitating the comparison to published findings with conventional analysis methods (Ravanfar et al., 2021; Stüber et al., 2016). We hypothesized that DGM areas intersecting multiple HA networks would have high iron levels relative to DGM areas intersecting only a single network, based on previous findings that most iron-modifying factors *increase* iron levels in healthy individuals (Aquino et al., 2009; Daugherty and Raz, 2013). We also hypothesized that identified networks would be differentially associated with demographic, clinical, and certain behavioral aspects, based on previous findings that DGM regions are differentially associated with these factors (Li et al., 2021; Pirpamer et al., 2016).

To answer the second and third questions, we tested the hypothesis that networks are altered in MS patients, as quantified by their loading coefficients using ICA decompositions from a cohort of MS patients and age- and sex-matched HCs. Additional regression analyses were performed between the disease-related networks and known iron-modifying behavioral factors as well as disease duration (“*dd*”), total T2 lesion volume, and Expanded Disability Status Scale (EDSS) score to relate these networks to potential underlying physiological mechanisms.

2.1 Participants and data collection

This retrospective, IRB-approved study involved two overlapping cohorts. The healthy aging (HA) cohort comprised 170 subjects without a clinically diagnosed neurological disease. The second cohort was previously described (Schweser et al., 2018), and comprised 120 patients with MS and 120 healthy controls (HCs): 40 patients with clinically isolated

syndrome (CIS) and 40 age- and sex-matched HCs, 40 patients with relapsing-remitting MS (RRMS) and 40 matched HCs, and 40 patients with secondary progressive MS (SPMS) with 40 matched HCs. A total of 74 HCs from the MS/HC cohort were also included in the HA cohort. The study was approved by the local ethical standards committee, and written informed consent was obtained from all participants according to the Declaration of Helsinki.

Demographic, clinical, and behavioral data were collected during an in-person interview and with additional standardized questionnaires. The full questionnaire form was previously published (Dolic et al., 2011). Details on age, sex, disease duration, and EDSS scores of the cohorts are provided in Table 1.

2.2 MRI and reconstruction

Imaging was performed at the same 3T scanner (Signa Excite HD 12.0; General Electric, Milwaukee, WI, USA) using an eight-channel head-and-neck coil and using the same three-dimensional gradient-echo sequence with first-order flow compensation in read and slice directions (matrix, 512 × 192 × 64; 0.5 × 1 × 2 mm; 12° flip; echo time, 22 ms; retention time, 40 ms; bandwidth, 13.89 kHz). Phase images were unwrapped (Abdul-Rahman et al., 2007), background field corrected (Li et al., 2011; Schweser et al., 2011), and converted into field maps, assuming zero-phase at TE=0 (Schweser et al., 2016). Susceptibility maps were calculated using homogeneity-enabled incremental dipole inversion with whole-brain referencing (Schweser et al., 2012). Susceptibility maps were normalized to a custom isotropic 1-mm^3 susceptibility brain template using advanced normalization tools (Fig. 2A) (Hanspach et al., 2017), which allowed for comparisons between subjects with different brain morphologies such as pediatric subjects and adults, and smoothed with a 1-mm^3 Gaussian kernel. This procedure was used because QSM provides much clearer delineation of the DGM structures than T_1-weighted images, allowing for higher accuracy registration in those areas (Hanspach et al., 2017). The following additional sequences were acquired during the same imaging session for all subjects: spin-echo T_1-weighted imaging (matrix, 256 mm × 192 mm; FOV, 256 mm × 192 mm; echo time, 16 ms; retention time, 600 ms); FLAIR (matrix, 256 mm × 192 mm; FOV, 256 mm × 192 mm; echo time, 120 ms; inversion time, 2100 ms; retention time, 8500 ms; flip angle, 90°; echo-train length, 24); dual fast spin-echo proton density- and T_2-weighted imaging (matrix, 256 mm × 192 mm; FOV, 256 mm × 192 mm; TE_1, 9 ms; TE_2, 98 ms; repetition time, 5300 ms; echo-train length, 14); and a 3D high-resolution $T1_w$ fast spoiled GRE sequence (flip echo time, 2.8 ms; inversion time, 900 ms; retention time, 5.9 ms; flip angle, 10°; isotropic 1 mm resolution).

2.3 ICA

ICA (FSL MELODIC [multivariate exploratory linear optimized decomposition into independent components]) was applied to each cohort to obtain networks of statistically independent source components with associated subject-specific weights (loading coefficients; see Fig. 1 and the Introduction section for a schematic and interpretation of the ICA decomposition process) (Beckmann and Smith, 2004). The number of components was set to 70 for comparability with previous studies (Douaud et al., 2014; Smith et al., 2009), and data were variance-normalized pre-ICA and mixture-modeled post-ICA. The

ICA decompositions were then prefiltered by searching for and excluding nonrepresentative subjects in the cohort, guided by outliers in the loading coefficients. Reasons for outliers were QSM reconstruction errors and extremely high DGM iron.

We were not able to identify clinical conditions explaining extreme iron load. Considering the inclusion criteria, we assumed the findings were related to unidentified, subclinical pathology, justifying exclusion from the HA cohort. A second decomposition was applied to the remaining subjects to give a final ICA decomposition.

2.4 Identification of DGM-associated networks in the HA cohort

Anatomical network associations were assessed using brain atlases non-linearly registered to the brain template, which were visually assessed for registration quality. HA cohort-derived networks associated with DGM regions (referred to as DGM networks) were identified by calculating average *Z*-scores in the whole thalamus, caudate, and putamen (Harvard-Oxford subcortical atlas) as well as in the subthalamic nucleus, substantia nigra, red nucleus, and globus pallidus interna (GP_i), and globus pallidus externa (AHEAD atlas). (Fig. 2B, subcortical atlas) (Alkemade et al., 2020; Desikan et al., 2006). Left and right hemispheres were considered separately due to previous reports of inter-hemispheric magnetic susceptibility differences in people with neurological disease (Xu et al., 2008) and in multiple sclerosis patients (Hagemeier et al., 2018a). DGM networks were those with an average absolute *Z*-score ($|Z_{av}|$) of > 4.05 across the whole area of one or more regions, corresponding to a *P* value of < 0.001 in two-tailed *t* tests with Bonferroni correction for 16 comparisons (regions) (Woo et al., 2014).

Additional anatomical relationships were analyzed by adding a cortical atlas (64 regions total) (Desikan et al., 2006), a thalamic subnuclei atlas (14 subregions total) (Najdenovska et al., 2018), a cerebellar gray matter atlas (28 regions) (Diedrichsen et al., 2009), and a white matter tract atlas (48 regions) (Mori et al., 2008). Percent overlaps were calculated between atlas subregions and the robust DGM networks (thresholding at $|Z_{av}| > 3.3$, corresponding to $P < 0.001$, two-tailed *t* tests).

2.5 Network robustness analysis and MS/HC network matching

The internal reproducibility (robustness) of each HA cohort DGM network was assessed by repeating source separation 20 times on subsets of 84 randomly sampled subjects with replacement. The DGM networks were then matched to the maximally Pearson-correlated counterpart in each iteration (based on vectorized *Z*-score maps) (Duann et al., 2003). The average of these correlations ($Corr_{av}$) was defined as network robustness. Low robustness was defined as a $Corr_{av}$ of < 0.3, moderate robustness was defined as a $Corr_{av}$ of > 0.3 and < 0.7, and strong robustness was defined as a $Corr_{av}$ of > 0.7 according to previous classifications (Dancey and Ready, 2007). Network robustness was visualized by calculating probability maps of the fraction of the 20 DGM network-matched ICA iterations that were significant ($|Z| > 3.3$) for each voxel.

A similar robustness analysis was performed for the additional MS/HC disease-associated networks (see section 2.8, “Comparisons of networks”, below). For these networks, source separation was repeated 20 times on random subsets of 120 subjects, with 20 subjects

randomly selected without replacement from each of the groups to ensure each group was represented in the final sample (CIS, RRMS, SPMS, CIS-HVs, RRMS-HVs, and SPMS-HVs).

Each HA cohort-derived DGM network was matched to an equivalent network in the MS/HC group by nonlinearly transforming both sets of Z-score maps to MNI152 space, calculating the Pearson correlation with each vectorized Z-score network map in the MS/HC group, and selecting the MS/HC network with the highest correlation coefficient (r_{max}). All HA DGM networks were included in this analysis, including networks with low robustness, to assess the specificity of HA cohort networks to the HA cohort and the specificity disease-associated networks to the MS/HC cohort (see section 2.8 “Comparisons of networks”, below). Similar to that for the robustness analysis, weakly matched was defined as a r_{max} of < 0.3, moderately matched was defined as a r_{max} of > 0.3 and < 0.7, and strongly matched was defined as a r_{max} of > 0.7. A similar matched procedure was applied in the reverse direction matching MS/HC disease-related networks to HA cohort networks to identify disease-specific networks.

2.6 Average susceptibility values in HA cohort DGM networks

Susceptibility values were averaged voxel-wise across subjects in the DGM subcortical atlas. Student’s t tests compared mean susceptibilities in subcortical atlas areas overlapping the network intersection (i.e., more than one network present) with those overlapping the disjoint portions of the networks (i.e., only a single network present; network threshold: $|Z| > 3.3$).

2.7 Multivariable regression for ICA networks

Linear regression models were conducted on a subset of 70 subjects from the HA cohort with available clinical data using the network loading coefficients as dependent variables. Six factors known to modify brain iron were chosen as independent variables based on available clinical data: age (Ashraf et al., 2018), sex (Ayton et al., 2020), systolic blood pressure (BP) (Li et al., 2021), BMI (Pirpamer et al., 2016), self-reported smoking status (Li et al., 2021; Pirpamer et al., 2016), and self-reported migraines (Kruit et al., 2009). An age-by-sex interaction (age × sex) was also included in the model (Bartzokis et al., 2007). In models with nonsignificant age × sex, the age × sex term was removed and the model was rerun.

Similar regression analyses were performed on disease-related DGM networks derived from the MS/HC cohort (see section 2.8, “Comparisons of networks”, below). In this regression, the disease duration (*dd*), expanded disability status scale (EDSS), and T2 total lesion volume (calculated using a semi-automated contouring/thresholding technique on FLAIR images as described previously (Zivadinov et al., 2001)) were used as independent variables in addition to the six factors included in the HA cohort regression (nine total independent variables).

Additional regression analyses were performed on a combined cohort of 184 patients and HCs from the MS/HC cohort who had available data. This regression included disease status interaction terms (age, sex, BMI, current smoking status, systolic BP, and migraine status)

and main effects of age, sex, BMI, current smoking status, systolic BP, and migraine status but excluded dd, EDSS, and T2 total lesion volume.

2.8 Comparisons of networks

In the main analysis, linear models were used to compare loading coefficients of MS/HC networks matched to the robust HA networks (DGM only) between disease groups (MS and HC) and MS subtypes (CIS, RRMS, and SPMS) while statistically adjusting for age and sex. For tests with significant disease group-by-MS subtype interactions, *post hoc* comparisons were conducted between MS patients and matched HCs for each MS subtype (i.e., patients with CIS vs. CIS-matched HCs, patients with RRMS vs. RRMS-matched HCs, and patients with SPMS vs. SPMS-matched HCs) and between MS subtype groups (i.e., patients with CIS vs. patients with RRMS, patients with CIS vs. patients with SPMS, and patients with RRMS vs. patients with SPMS). Exploratory analyses involved the same procedure for the remaining networks from the MS/HC cohort that were associated with at least one DGM region (> 5% overlap). Robustness of the main and interaction effects was tested by adding BMI, systolic BP, current smoking status, and migraine status as covariates and retesting for statistical significance.

2.9 ROI-based detection of disease effects and exploratory multivariate regression

For each subject in the MS/HC cohort, average susceptibility values were calculated within each DGM atlas region and the two pulvinar atlas regions, and then averaged across hemispheres (nine total ROIs). Linear models were used to compare the average susceptibility in each ROI between disease groups (MS and HC) and MS subtypes (CIS, RRMS, and SPMS) while statistically adjusting for age and sex. For tests with significant disease group-by-MS subtype interactions, *post hoc* comparisons were conducted using the same contrasts described in Section 2.8, “Comparison of networks”. Robustness of the main and interaction effects was tested by adding BMI, systolic BP, current smoking status, and migraine status as covariates and retesting for statistical significance.

Exploratory regression models were applied to each ROI with significant main effect of disease status or significant disease group-by-MS subtype using average susceptibility as the dependent variable and the same independent variables as used for the disease-related DGM network regression (see Section 2.7, “Multivariable regression for ICA networks”). Further exploratory regression analyses were conducted on the caudate and pulvinar ROIs, due to their direct anatomical comparability to the Pulvinar and Caudate Networks.

2.10 Statistics for regression analyses and disease group comparisons

Statistical analyses were conducted using SPSS (27.0; IBM, Armonk, NY). Model assumptions were assessed using standard diagnostic plots.

Bonferroni corrections were applied to the average susceptibility value comparisons between overlapping and nonoverlapping network areas. In linear models for disease group comparisons, the significance levels ($P < 0.05$) for the main effect of disease group and for the disease group-by-MS subtype interaction were Bonferroni corrected for 18 comparisons (disease group main effect and disease group-by-MS subtype interaction effect for the two

main comparisons and 7 additional exploratory linear models). Tukey's least significant difference tests were used for *post hoc* pairwise comparisons for significant disease group-by-MS subtype interactions. ROI-based disease group comparisons were Bonferroni corrected for 18 comparisons (disease group main effect and disease group-by-MS subtype interaction effect for nine ROIs), and Tukey's least significant difference tests were used for *post hoc* pairwise comparisons for significant disease group-by-MS subtype interactions.

Regression analysis were not corrected for multiple comparisons due to the exploratory nature of the analysis (Althouse, 2016).

3. Results

3.1 Five DGM networks linked to healthy aging

In total, four non-representative individuals were excluded from the HA cohort. Figure 3 shows the five HA cohort DGM networks (Dorsal Striatum, Brainstem, GP_i, Thalamus, and Cerebellar Networks) that significantly overlapped at least one DGM region.

The Dorsal Striatum and GP_i Networks had moderate-to-high robustness (i.e., anatomical consistency; $Corr_{av}$ = 0.81 and 0.56, respectively), whereas the Brainstem, Thalamus, and Cerebellar Networks had low robustness ($Corr_{av}$ = 0.27, 0.21, and 0.22, respectively). Figure 4 shows the areas that were most consistently associated with each network by visualizing the fraction of the 20 DGM network-matched ICA iterations that were significant ($|Z| > 3.3$) at each voxel.

Figure 5A shows the volume overlap (> 5% only) of the two highly robust DGM networks in different anatomical areas. The Dorsal Striatum Network had > 5% overlap with every structure in the combined DGM atlas as well as with several regions from the thalamic atlas (ventral-lateral-dorsal nucleus and central-lateral + lateral-posterior + medial-pulvinar nuclei), cerebellar gray matter atlas (VI cerebellum and vermis VIIIa + IX + X cerebellum), and white matter atlas (cerebellar peduncle, anterior and posterior limbs of the internal capsule, external capsule, fornix, and superior frontal-occipital fasciculus). The GP_i Network had > 5% overlap with every area of the combined DGM atlas except the left caudate, left red nucleus, right putamen, and left and right whole thalami as well as with several regions from the white matter atlas (cerebellar peduncle, anterior limb of the internal capsule, and tapetum).

3.2 Regions of network overlap have increased susceptibility

In the DGM of the HA cohort, areas intersecting both the Dorsal Striatum Network and the GP_i Network had higher mean susceptibility values than areas intersecting only one of the networks (e.g., Dorsal Striatum Network but not GP_i Network) (Fig. 5B; $P < 0.001$ for both comparisons).

3.3 Robust HA networks distinctly linked to age, sex, and migraine

Regression results for the HA cohort are summarized in Table 2 (left). The Dorsal Striatum Network was negatively associated with age × sex ($P = 0.021$) and positively associated with

age ($P = 0.004$) and male sex ($P = 0.022$). The GP_i Network was positively associated with age ($P = 0.004$) and self-reported migraines ($P = 0.022$) (see also Fig. 7).

3.4 MS affects the GP_i Network and three additional robust MS/HC cohort networks

In total, 2 MS patients and 5 HCs were excluded for the final ICA decomposition for the MS/HC cohort. A disease group comparison analysis, with between-group age and sex differences statistically corrected by including them as covariates, revealed a main effect of disease status (MS vs. HC) for four of the nine MS/HC DGM-associated networks: the GP_i and MS Pulvinar Networks and two additional DGM-associated networks (MS Mesencephalon and MS Caudate Networks; all $P < 0.02$, Bonferroni corrected). A main effect of disease status remained significant with the addition of BMI, systolic BP, current smoking status, and migraine status as covariates for MS GP_i, Caudate, and Mesencephalon Networks ($P < 0.02$, Bonferroni corrected) but not for the Pulvinar Network ($P = 0.054$, Bonferroni corrected).

A disease group-by-MS subtype interaction effect was significant for the MS Pulvinar Network ($P < 0.02$, Bonferroni corrected). Tukey's *post hoc* least significant difference tests of the MS Pulvinar Network showed that the mean-adjusted loading coefficients were significantly lower for patients with SPMS than for SPMS-matched HCs (−0.697 vs. 0.345; $P < 0.001$), but there was no significant difference between patients with CIS and CIS-matched HCs (0.117 vs. 0.075; $P = 0.833$) or between patients with RRMS and RRMS-matched HCs (−0.017 vs. 0.258; $P = 0.180$). Additionally, mean-adjusted loading coefficients for the MS Pulvinar Network were significantly lower for patients with SPMS than for patients with CIS (−0.697 vs. 0.117; $P < 0.001$) and patients with RRMS (−0.697 vs. −0.017; $P = 0.001$), but were not different between patients with RRMS and those with CIS (−0.017 vs 0.117; $P = 0.512$). The interaction effect did not remain significant with the addition of BMI, systolic BP, current smoking status, and migraine status as covariates ($P > 0.1$).

Robustness analysis showed that each of the three additional disease-associated MS/HC cohort networks had moderate to high robustness ($Corr_{av} = 0.53$, 0.73, and 0.49 for the Mesencephalon, Pulvinar, and Caudate Networks, respectively).

3.5 MS networks have distinct anatomical associations

Figure 6B shows the volume overlap (> 5%) of the three additional MS networks (MS Mesencephalon, Pulvinar, and Caudate Networks) in different anatomical areas. The MS Mesencephalon Network had > 5% overlap with several white matter structures, including the pontine crossing tract and the left and right corticospinal tracts and superior cerebellar peduncles, and with the left and right red nuclei, substantia nigra, and cerebellar I–IV. The MS Pulvinar Network overlapped primarily with the left and right pulvinar of the thalamus. The MS Caudate Network overlapped with the left and right caudate and the left and right anterior limbs of the internal capsule.

The Dorsal Striatum and GP_i Networks in the HA cohort (Fig. 3) were moderately matched to similar networks from the MS/HC cohort ($r_{max} = 0.540$ and 0.541, respectively) (Fig. 6A), the Thalamus Network was moderately matched to the Pulvinar Network ($r_{max} = 0.407$)

(Fig. 6B), and the Brainstem and Cerebellar Networks matched only weakly to MS/HC cohort networks (r_{max} = 0.191 and 0.221, respectively).

The MS Caudate Networks were moderately matched to a network from the HA cohort (r_{max} = 0.386). By contrast, the MS Mesencephalon Network was weakly matched (r_{max} = 0.207). Cereb. = cerebellar; Front-Occ. Fasc. = fronto-occipital fasciculus; Int. Cap. = internal capsule; Sup. = superior; VL = ventral-lateral.

3.6 MS networks distinctly associated with disease duration and lesion burden

The MS Pulvinar Network had a negative association with *dd* (P = 0.005), whereas the MS Caudate and Mesencephalon Networks had positive associations with total T2 lesion volume (P = 0.018 and 0.013, respectively) (Table 2, right). These associations are visualized as a schematic in Fig. 7. The GP_i Network was not associated with any of the variables in the MS-only regression, in contrast to the association found in the regression analysis for the HA cohort.

Additional regression analyses with the full MS/HC cohort showed significant interaction effects of disease status by age for the MS GP_i (P = 0.023) and Pulvinar (P = 0.002) Networks, and disease status by BMI for the MS Mesencephalon Network (P = 0.026).

3.7 ROI-based analysis has lower sensitivity to disease effects and disease-related factors

A disease group comparison analysis showed that the putamen, caudate, and GP_i had main effects of disease status (MS vs. HC) with $P < 0.05$. However, only putamen ROI survived Bonferroni correction for multiple comparisons (after Bonferroni correction, $P < 0.001$ for putamen and P = 0.06534 and 0.774 for caudate and GP_i, respectively). The putamen ROI main effect of disease status remained significant with the addition of BMI, systolic BP, current smoking status, and migraine status as covariates (P = 0.036 Bonferroni corrected). The thalamus and GP_e ROIs had disease group-by-MS subtype interaction effects with $P < 0.05$, but neither effect survived correction for multiple comparisons (P > 0.4 Bonferroni corrected for both).

Exploratory regression analysis (Tab. 3) showed the putamen ROI had a positive association with age (P = 0.001). Additional exploratory regression analysis showed a negative association between smoking status and the pulvinar ROI (P = 0.036). No associations were seen between the caudate ROI and any of the independent variables ($P > 0.05$).

4. Discussion

The results of this study show that DGM iron variation in healthy aging is organized into two robust, partially-overlapping networks which are differentially associated with demographic and clinical factors (i.e. age by sex interaction and self-reported migraine status). We found that these networks were differentially affected by MS disease status, and discovered three additional MS-related networks. These networks allowed for higher sensitivity in detecting MS disease effects when compared to a ROI-based analysis on the same subjects.

4.1 DGM networks detect MS disease effects with higher sensitivity than ROI-based analyses

ICA analysis revealed four networks that were significantly associated with MS. In contrast, only the putamen ROI was associated with MS disease status in the ROI-based analysis, despite using the same set of subjects and having the same alpha level as the ICA analysis ($P < 0.05$ corrected for eighteen comparisons). Notably, the Pulvinar and Caudate Networks loading coefficients were significantly associated with MS whereas the pulvinar and caudate ROI mean susceptibility values were not, despite covering similar anatomical areas. This finding is likely due to the ICA analysis separating the disease effects from the effects of healthy aging, as evidenced by the presence of the Dorsal Striatum Network, which covers the pulvinar and caudate, in the MS/HC cohort ICA decomposition. Another contributing factor may be that the ICA procedure separated artifacts and noise into separated components from the healthy aging and disease-associated components. This feature of ICA is widely used in fMRI studies and may have similar effects here (Salimi-Khorshidi et al., 2014). Additionally, unlike the Pulvinar and Caudate Networks, exploratory regression analysis for the pulvinar and caudate ROIs did not show any significant associations to disease duration or T2 lesion volume. These results suggest that the ICA analysis allows for higher sensitivity in detecting disease effects than ROI analyses and highlight the advantage of the ICA approach for studying specific disease factors.

4.2 Independent patterns of susceptibility change and no support for accelerated iron aging in patients with MS

Both the Dorsal Striatum and GP_i Networks showed age associations, which we interpret as evidence of two separate naturally occurring, age-related iron/myelin networks on the basis of the differential effects of age × sex in the two networks. Specifically, the results indicate the Dorsal Striatum Network, but not the GP_i Network, undergoes iron changes in response to potential factors such as menstruation and menopause, which are specific to females and have been shown to alter peripheral blood iron levels (Whitfield et al., 2003). The differential effect of age × sex suggests that these networks may be governed by different biological processes.

Another piece of evidence for independent processes of iron change in the two robust DGM networks comes from the differential effect of MS disease status on the matched Dorsal Striatum and GP_i Networks from the MS/HC cohort. There was a significant effect of disease status, independent of age and sex, in the GP_i Network but not in the Dorsal Striatum Network. The processes that underlie this effect are not clear. The positive association between the GP_i Network and self-reported migraine status is consistent with previously reports of increased iron in the globus pallidus and red nucleus (Kruit et al., 2009). It is unlikely that migraine status contributed to GP_i Network differences between patients with MS and HCs because the prevalence was similar between the two groups (18.6% for HA cohort, 12.0% for MS-only cohort) and there was no disease status-by-migraine interaction effect in the regression analysis. Confirmatory studies showing that the GP_i Network is enhanced in patients clinically diagnosed with migraines compared to that in healthy controls would confirm this link.

We validated our hypothesis that healthy individuals have higher susceptibility values in DGM areas overlapping multiple networks (i.e., the Dorsal Striatum and GP_i Networks) than in regions in only one of those networks. These overlapping areas, including the red nucleus and substantia nigra, are well known to have higher iron levels than other DGM regions. The processes underlying relatively high iron accumulation in these regions with regard to aging and disease are currently unknown (Ramos et al., 2014; Snyder and Connor, 2009). When combined with the evidence described above, it is possible that iron levels are comparatively high in these regions because they involve multiple independent processes of iron accumulation, represented in our study as separate overlapping iron networks (Fig. 1C and 3A). However, histological and pathological studies comparing these networks are needed to confirm this hypothesis.

It was previously suggested that MS and other neurodegenerative diseases accelerate naturally occurring biological processes underlying healthy aging (Franke and Gaser, 2019), and MRI studies indicate an increased morphological “brain age” in individuals with MS (Cole et al., 2020; Høgestøl et al., 2019). Here, we did not find evidence for the enhancement of aging-related processes in patients with MS that manifested as altered susceptibility in MRI to support this hypothesis. On the contrary, our results suggest that the normal aging-related changes are disrupted in MS, not accelerated, because the GP_i Network was positively associated with age in the HA cohort but not in the MS cohort. This may indicate a dissociation between aging-related atrophy and iron homeostatic processes in MS, i.e., aging-related atrophy is accelerated whereas aging-related iron homeostasis is disrupted, resulting in a decline in total brain iron content in MS (Schweser et al., 2021). Further studies on the relationship between MS-associated telomere shortening and disease-related iron networks are needed (Hecker et al., 2021).

The high robustness of the Dorsal Striatum and GP_i Networks makes them good targets for future studies. They may be used to study other clinical and behavioral factors that affect brain iron, such as diabetes mellitus, or to study the effects of other neurological disorders such as Parkinson’s disease.

4.3 Additional MS networks suggest distinct disease processes in different regions

The results from the analysis of MS-related DGM networks are consistent with previous studies showing iron alterations in the caudate (Hagemeier et al., 2018b), thalamus and pulvinar (Khalil et al., 2015; Zivadinov et al., 2018), red nucleus (Blazejewska et al., 2015), and substantia nigra (Blazejewska et al., 2015). These areas represent four statistically independent networks rather than a single network. This suggests that MS affects these networks differentially, potentially through distinct iron- and myelin-related disease processes. Note that each of the comparisons between MS patients and HCs and between MS subtypes was corrected for age and sex, so that any remaining effects were specific to disease and not caused by e.g. increased age in patients with SPMS compare to patients with CIS. Robustness analysis confirmed that these networks had moderate to high internal reproducibility, indicating they are reliable targets for future studies. Additionally, the robustness analyses used 120 subjects (half of the full sample), showing that these networks were not simply pieces of the HA cohort networks that had been fragmented due

to increased sample size (compared to the 166 subjects used in the HA full cohort source separation). Future studies will further test the relationship between these iron networks and additional clinical factors, such as diabetes status, and markers of clinical outcomes such as cognitive tests (e.g., paced auditory serial addition test) (Macías Islas and Ciampi, 2019).

4.4 Support for Wallerian degeneration as a cause of caudate atrophy

Studies of patients with MS have shown evidence of internal capsule lesions and axonal damage and, in separate studies, selective caudate atrophy (Bermel et al., 2003; Dalton et al., 2012; Lee et al., 2000). In our study, the anterior limb of internal capsule and caudate appeared together in a single disease-related network, the MS caudate network. Both areas had positive susceptibility associations within the network, likely because of increased iron concentration in the caudate and demyelination in the anterior limb of internal capsule (Lee et al., 2000). Additionally, the MS caudate network was positively associated with T2 lesion volume. These results support the previously-proposed hypothesis that caudate-specific atrophy is caused by Wallerian degeneration in associated white matter tracts (i.e. white matter connections between the lentiform and caudate nuclei as contained in the anterior limb of internal capsule) (Bermel et al., 2003). It should be noted that this interpretation is potentially limited by the relatively low resolution of the QSM images and the close proximity of the caudate and internal capsule. However, visual inspection of the MS Caudate Network confirmed that it extended into the anterior limb of the internal capsule, indicating that this association was not entirely accounted for by atlas misalignment.

4.5 Susceptibility decrease in the pulvinar is independent of the optic pathway

The MS Pulvinar Network was moderately matched to the Thalamus Network (0.407). However, the Thalamus Network had low robustness (i.e., high anatomical variation), with only a small area (13 voxels) appearing in half or more of the 20 DGM network-matched ICA iterations. Low Thalamus Network robustness could occur because thalamic subnuclei are weakly associated with each other but have strong heterogeneous connectivity to the cerebral cortex (Fama and Sullivan, 2015). These subnuclei may be subjected to different iron-related factors and metabolic demands (Cho et al., 2011). Thus, the thalamus may not act as a single cohesive unit with regard to its iron behavior and complicate attempts to disentangle specific networks with ICA. Indeed, thalamic subnuclei have different iron-related effects in MS (Schweser et al., 2018). Whatever the cause, low robustness weakens the claim that two networks derived from separate subject groups are manifestations of the same network, and so it remains unclear whether the MS Pulvinar Network is disease specific or is also present in the HA cohort.

A previous ROI-based study using the same cohort found that susceptibility decreases in the pulvinar with increases in disease duration and suggested the effect was secondary to damage elsewhere in the optic pathway (Schweser et al., 2018). The null association between T2 lesion volume and MS Pulvinar Network loading coefficients ($P = 0.717$) does not support this hypothesis. However, this lack of relationship may reflect a poor association between overall lesion burden and optic pathway lesion burden, because only a small fraction of the overall lesion burden affects the optic nerve. Other contradicting evidence comes from the pulvinar specificity of the MS Pulvinar Network. Despite the strong

connections between the pulvinar and other optic processing areas such as the occipital cortex, statistical independence of the MS Pulvinar Network implies that iron and myelin in these other areas are not altered in the same way as in the pulvinar. Future QSM studies could test this theory by comparing the longitudinal susceptibility trajectories of these areas. Additionally, postmortem histological comparisons between these brain regions would confirm whether similar disease processes occur in these areas. Instead, the strong negative effect of *dd* indicates that the MS-related pulvinar susceptibility decrease may be due to local disease processes, such as diffuse microglial activation in the thalamus, as shown previously (Rissanen et al., 2018). Nevertheless, it is possible that injury to optic pathways also influences the pulvinar but to a lesser extent than previously thought (Zivadinov et al., 2014).

4.6 Mesencephalon and brainstem networks differentially affected

The MS Mesencephalon Network was associated with the brainstem and select cerebellar areas. However, it was weakly matched with the Brainstem Network, indicating these two networks are composed of different structures. The positive association between T2 lesion volume potentially points to demyelination as the basis of this network. It is possible that spinal cord lesions also influence this network, although spinal cord MRI scans were not available for the patients in this study.

4.7 Limitations and future directions

The interpretation of QSM studies is generally limited by the fact that both iron and myelin influence magnetic susceptibility. Increased iron levels and demyelination both increase susceptibility, whereas decreased iron levels and increased myelin decrease susceptibility. Other biological factors such as calcium can also affect susceptibility values but likely to a lesser extent in healthy individuals and patients with MS (Schweser et al., 2018). The interpretation of susceptibility values can be aided by comparisons to histological studies or to other iron-sensitive MRI techniques such as transverse relaxation rate (R_2*), which is affected by myelin in the opposite way (i.e., increased myelin increases R_2* values) (Hametner et al., 2018). With these considerations, any interpretation of susceptibility values needs to carefully consider modifying factors and the anatomical regions analyzed. Extension of the ICA method to include other quantitative MRI metrics such as R2* through the use of linked ICA could enable the separation of iron and myelin networks and provide even higher specificity and sensitivity for evaluating brain iron (Douaud et al., 2014). Alternatively, recently introduced methods to separate paramagnetic and diamagnetic sources (Chen et al., 2021; Shin et al., 2021) could be applied prior to ICA to a similar effect.

The ability of ICA to detect networks depends on the number of subjects, the number of components used in the ICA decomposition, and the sensitivity of the imaging technique itself. For example, in functional MRI-based ICA analysis of the default mode network, increasing the number of components for the ICA decomposition can split the default mode network into subnetworks (Manoliu et al., 2013). Future studies could test how altering the number of components affects these networks.

Although visual analysis showed excellent registration of the anatomical atlases to the subject template, the relatively large slice thickness (2mm) may have limited accurate assessment of smaller DGM structures such as the globus pallidus interna or the substantia nigra. This consideration also limits conclusions about network associations of neighboring structures, such as the caudate and internal capsule. Future studies could address this issue with higher resolution scan sequences. However, this limitation also highlights a benefit of the ICA approach, which does not require atlases to generate the networks, unlike ROI analyses in which manual or automatic anatomical segmentation is necessary.

Our preliminary exploratory study provides unique insight into brain iron physiology but was limited by the cross-sectional retrospective design. Future studies should include a larger number of subjects with migraines and smoking exposure and analyze other variables known to affect brain iron, such as apolipoprotein E gene mutations (Yim et al., 2022). A longitudinal study design would enable analysis of the susceptibility networks over time, which may better reveal individual differences in the networks than the between-subjects design used in the present study.

The methodology presented here provides a step forward in studies of brain iron physiology, which were previously restricted to voxel- or ROI-based analyses. Given the ability of ICA to separate independent sources, ICA can be applied to QSM images to potentially filter out nonrelevant susceptibility variations and detect disease-relevant patterns with higher specificity. The methodology of this study could also be applied to other diseases with presumed iron dyshomeostasis, such as Parkinson's disease, to analyze susceptibility networks occurring in other disease contexts. Future studies could also analyze networks not associated with the DGM, which would be most easily interpreted if combined with methods to separate the effects of iron and myelin (Chen et al., 2021; Shin et al., 2021). As we have shown, the proposed methodology produces networks that are highly internally reproducible and could be used as biomarkers for disease progression or to quantify the effects of disease-modifying therapies. Just as the application of ICA to functional and anatomical MRI images has revealed important scientific knowledge about brain function and structure (Garrity et al., 2007; McKeown et al., 2003), the proposed technique may reveal equally important knowledge about brain iron physiology.

5. Conclusion

Our work introduces a novel approach to separate independent patterns of susceptibility change to understand the variation in magnetic susceptibility among subjects. We found two internally reproducible covarying networks of DGM brain iron associated with age, which are affected differently in patients with MS than in controls. When applied to a combined cohort of patients with MS and HVs, the ICA network framework was more sensitive to disease-related effects than a ROI-based approach. Our results provide evidence that several known disease-related effects act independently of one another, such as increased DGM susceptibility in the caudate and decreased susceptibility in the pulvinar. Conversely, we also showed that several MS-related findings reported in other studies are related and may be caused by the same disease process, e.g., internal capsule myelin damage and increased caudate iron concentrations. This study advances knowledge of healthy brain iron

physiology and MS pathophysiology, and provides a conceptual and technical framework for future studies to build on.

Acknowledgments

The authors would like to thank Zachary Weinstock, Alexander Bartnik, and Dr. Karen Dietz for their feedback on the manuscript.

Funding

Research reported in this publication was supported by grants from the National Institutes of Health (R01NS114227 from the National Institute of Neurological Disorders and Stroke and UL1TR001412 from the National Center for Advancing Translational Sciences). The content is solely the responsibility of the authors and does not necessarily represent the official views of the National Institutes of Health.

Competing interests

Bianca Weinstock-Guttman has participated in speakers bureaus for, served as a consultant for, and/or received research support from Biogen, EMD Serono, Novartis, Genentech, Celgene/Bristol Meyers Squibb, Sanofi & Genzyme, Janssen, Horizon, Bayer, and LabCorp. Dr. Weinstock-Guttman also serves on the editorial board for BMJ Neurology, Children, CNS Drugs, MS International, and Frontiers Epidemiology.

Robert Zivadinov has received personal compensation from Bristol Myers Squibb, EMD Serono, Sanofi, Keystone Heart, Protembis, and Novartis for speaking and consultant fees and has received financial support for research activities from Sanofi, Novartis, Bristol Myers Squibb, Octave, Mapi Pharma, Keystone Heart, Protembis, and V-WAVE Medical.

References

Abdul-Rahman HS, Gdeisat MA, Burton DR, Lalor MJ, Lilley F, Moore CJ, 2007. Fast and robust three-dimensional best path phase unwrapping algorithm. Appl Opt 46, 6623–6635. 10.1364/ao.46.006623 [PubMed: 17846656]

Acosta-Cabronero J, Cardenas-Blanco A, Betts MJ, Butryn M, Valdes-Herrera JP, Galazky I, Nestor PJ, 2017. The whole-brain pattern of magnetic susceptibility perturbations in Parkinson's disease. Brain 140, 118–131. 10.1093/brain/aww278 [PubMed: 27836833]

Alkemade A, Mulder MJ, Groot JM, Isaacs BR, van Berendonk N, Lute N, Isherwood SJ, Bazin P-L, Forstmann BU, 2020. The Amsterdam Ultra-high field adult lifespan database (AHEAD): A freely available multimodal 7 Tesla submillimeter magnetic resonance imaging database. NeuroImage 221, 117200. 10.1016/j.neuroimage.2020.117200 [PubMed: 32745682]

Althouse AD, 2016. Adjust for Multiple Comparisons? It's Not That Simple. The Annals of Thoracic Surgery 101, 1644–1645. 10.1016/j.athoracsur.2015.11.024 [PubMed: 27106412]

Aquino D, Bizzi A, Grisoli M, Garavaglia B, Bruzzone MG, Nardocci N, Savoiardo M, Chiapparini L, 2009. Age-related iron deposition in the basal ganglia: quantitative analysis in healthy subjects. Radiology 252, 165–172. 10.1148/radiol.2522081399 [PubMed: 19561255]

Ashraf A, Clark M, So P-W, 2018. The Aging of Iron Man. Front Aging Neurosci 10, 65. 10.3389/fnagi.2018.00065 [PubMed: 29593525]

Ayton S, Wang Y, Diouf I, Schneider JA, Brockman J, Morris MC, Bush AI, 2020. Brain iron is associated with accelerated cognitive decline in people with Alzheimer pathology. Mol Psychiatry 25, 2932–2941. 10.1038/s41380-019-0375-7 [PubMed: 30778133]

Bakshi R, Shaikh ZA, Janardhan V, 2000. MRI T2 shortening ('black T2') in multiple sclerosis: frequency, location, and clinical correlation. NeuroReport 11, 15–21. [PubMed: 10683822]

Bartzokis G, Tishler TA, Lu PH, Villablanca P, Altshuler LL, Carter M, Huang D, Edwards N, Mintz J, 2007. Brain ferritin iron may influence age- and gender-related risks of neurodegeneration. Neurobiol Aging 28, 414–423. 10.1016/j.neurobiolaging.2006.02.005 [PubMed: 16563566]

Beckmann CF, Smith SM, 2004. Probabilistic independent component analysis for functional magnetic resonance imaging. IEEE Trans Med Imaging 23, 137–152. 10.1109/TMI.2003.822821 [PubMed: 14964560]

Bermel RA, Innus MD, Tjoa CW, Bakshi R, 2003. Selective caudate atrophy in multiple sclerosis: a 3D MRI parcellation study. Neuroreport 14, 335–339. 10.1097/00001756-200303030-00008 [PubMed: 12634479]

Blazejewska AI, Al-Radaideh AM, Wharton S, Lim SY, Bowtell RW, Constantinescu CS, Gowland PA, 2015. Increase in the iron content of the substantia nigra and red nucleus in multiple sclerosis and clinically isolated syndrome: a 7 Tesla MRI study. J Magn Reson Imaging 41, 1065–1070. 10.1002/jmri.24644 [PubMed: 24841344]

Chen J, Gong N-J, Chaim KT, Otaduy MCG, Liu C, 2021. Decompose quantitative susceptibility mapping (QSM) to sub-voxel diamagnetic and paramagnetic components based on gradient-echo MRI data. NeuroImage 242, 118477. 10.1016/j.neuroimage.2021.118477 [PubMed: 34403742]

Cho Z-H, Son Y-D, Kim H-K, Kim N-B, Choi E-J, Lee S-Y, Chi J-G, Park C-W, Kim Y-B, Ogawa S, 2011. Observation of Glucose Metabolism in the Thalamic Nuclei by Fusion PET/MRI. Journal of Nuclear Medicine 52, 401–404. 10.2967/jnumed.110.081281 [PubMed: 21321261]

Cole JH, Raffel J, Friede T, Eshaghi A, Brownlee WJ, Chard D, De Stefano N, Enzinger C, Pirpamer L, Filippi M, Gasperini C, Rocca MA, Rovira A, Ruggieri S, Sastre-Garriga J, Stromillo ML, Uitdehaag BMJ, Vrenken H, Barkhof F, Nicholas R, Ciccarelli O, MAGNIMS study group, 2020. Longitudinal Assessment of Multiple Sclerosis with the Brain-Age Paradigm. Ann Neurol 88, 93–105. 10.1002/ana.25746 [PubMed: 32285956]

Comon P, 1994. Independent component analysis, A new concept? Signal Processing, Higher Order Statistics 36, 287–314. 10.1016/0165-1684(94)90029-9

Connor JR, Menzies SL, 1996. Relationship of iron to oligondendrocytes and myelination. Glia 17, 83–93. 10.1002/(SICI)1098-1136(199606)17:2<83::AID-GLIA1>3.0.CO;2-7 [PubMed: 8776576]

Dalton CM, Bodini B, Samson RS, Battaglini M, Fisniku LK, Thompson AJ, Ciccarelli O, Miller DH, Chard DT, 2012. Brain lesion location and clinical status 20 years after a diagnosis of clinically isolated syndrome suggestive of multiple sclerosis. Mult Scler 18, 322–328. 10.1177/1352458511420269 [PubMed: 21878451]

Dancey CP, Ready J, 2007. Statistics Without Maths for Psychology. Pearson Eduction.

Daugherty A, Raz N, 2013. Age-related differences in iron content of subcortical nuclei observed in vivo: a meta-analysis. Neuroimage 70, 113–121. 10.1016/j.neuroimage.2012.12.040 [PubMed: 23277110]

Desikan RS, Ségonne F, Fischl B, Quinn BT, Dickerson BC, Blacker D, Buckner RL, Dale AM, Maguire RP, Hyman BT, Albert MS, Killiany RJ, 2006. An automated labeling system for subdividing the human cerebral cortex on MRI scans into gyral based regions of interest. Neuroimage 31, 968–980. 10.1016/j.neuroimage.2006.01.021 [PubMed: 16530430]

Diedrichsen J, Balsters JH, Flavell J, Cussans E, Ramnani N, 2009. A probabilistic MR atlas of the human cerebellum. Neuroimage 46, 39–46. 10.1016/j.neuroimage.2009.01.045 [PubMed: 19457380]

Dixon SJ, Stockwell BR, 2014. The role of iron and reactive oxygen species in cell death. Nat Chem Biol 10, 9–17. 10.1038/nchembio.1416 [PubMed: 24346035]

Dolic K, Weinstock-Guttman B, Marr K, Valnarov V, Carl E, Hagemeier J, Brooks C, Kilanowski C, Hojnacki D, Ramanathan M, Zivadinov R, 2011. Risk factors for chronic cerebrospinal venous insufficiency (CCSVI) in a large cohort of volunteers. PLoS One 6, e28062. 10.1371/journal.pone.0028062 [PubMed: 22140507]

Douaud G, Groves AR, Tamnes CK, Westlye LT, Duff EP, Engvig A, Walhovd KB, James A, Gass A, Monsch AU, Matthews PM, Fjell AM, Smith SM, Johansen-Berg H, 2014. A common brain network links development, aging, and vulnerability to disease. Proc Natl Acad Sci U S A 111, 17648–17653. 10.1073/pnas.1410378111 [PubMed: 25422429]

Duann J, Jung T, Makeig S, Sejnowski TJ, 2003. Consistency of infomax ICA decomposition of functional brain imaging data, in: In Proceedings of the Fourth International Workshop on Independent Component Analysis and Blind Signal Separation. pp. 289–294.

Fama R, Sullivan EV, 2015. Thalamic structures and associated cognitive functions: Relations with age and aging. Neurosci Biobehav Rev 54, 29–37. 10.1016/j.neubiorev.2015.03.008 [PubMed: 25862940]

Franke K, Gaser C, 2019. Ten Years of BrainAGE as a Neuroimaging Biomarker of Brain Aging: What Insights Have We Gained? Front Neurol 10, 789. 10.3389/fneur.2019.00789 [PubMed: 31474922]

Garrity AG, Pearlson GD, McKiernan K, Lloyd D, Kiehl KA, Calhoun VD, 2007. Aberrant "default mode" functional connectivity in schizophrenia. Am J Psychiatry 164, 450–457. 10.1176/ajp.2007.164.3.450 [PubMed: 17329470]

Gillen KM, Mubarak M, Nguyen TD, Pitt D, 2018. Significance and In Vivo Detection of Iron-Laden Microglia in White Matter Multiple Sclerosis Lesions. Front Immunol 9, 255. 10.3389/fimmu.2018.00255 [PubMed: 29515576]

Hagemeier J, Ramanathan M, Schweser F, Dwyer MG, Lin F, Bergsland N, Weinstock-Guttman B, Zivadinov R, 2018a. Iron-related gene variants and brain iron in multiple sclerosis and healthy individuals. NeuroImage: Clinical 17, 530–540. 10.1016/j.nicl.2017.11.003 [PubMed: 29201641]

Hagemeier J, Zivadinov R, Dwyer MG, Polak P, Bergsland N, Weinstock-Guttman B, Zalis J, Deistung A, Reichenbach JR, Schweser F, 2018b. Changes of deep gray matter magnetic susceptibility over 2years in multiple sclerosis and healthy control brain. NeuroImage: Clinical 18, 1007–1016. 10.1016/j.nicl.2017.04.008 [PubMed: 29868452]

Hallgren B, Sourander P, 1958. The effect of age on the non-haemin iron in the human brain. J Neurochem 3, 41–51. 10.1111/j.1471-4159.1958.tb12607.x [PubMed: 13611557]

Hametner S, Endmayr V, Deistung A, Palmrich P, Prihoda M, Haimburger E, Menard C, Feng X, Haider T, Leisser M, Köck U, Kaider A, Höftberger R, Robinson S, Reichenbach JR, Lassmann H, Traxler H, Trattnig S, Grabner G, 2018. The influence of brain iron and myelin on magnetic susceptibility and effective transverse relaxation - A biochemical and histological validation study. NeuroImage 179, 117–133. 10.1016/j.neuroimage.2018.06.007 [PubMed: 29890327]

Hametner S, Wimmer I, Haider L, Pfeifenbring S, Brück W, Lassmann H, 2013. Iron and neurodegeneration in the multiple sclerosis brain. Ann Neurol 74, 848–861. 10.1002/ana.23974 [PubMed: 23868451]

Hanspach J, Dwyer MG, Bergsland NP, Feng X, Hagemeier J, Bertolino N, Polak P, Reichenbach JR, Zivadinov R, Schweser F, 2017. Methods for the computation of templates from quantitative magnetic susceptibility maps (QSM): Toward improved atlas- and voxel-based analyses (VBA). J Magn Reson Imaging 46, 1474–1484. 10.1002/jmri.25671 [PubMed: 28263417]

Hecker M, Fitzner B, Jäger K, Bühring J, Schwartz M, Hartmann A, Walter M, Zettl UK, 2021. Leukocyte Telomere Length in Patients with Multiple Sclerosis and Its Association with Clinical Phenotypes. Mol Neurobiol 58, 2886–2896. 10.1007/s12035-021-02315-y [PubMed: 33547621]

Høgestøl EA, Kaufmann T, Nygaard GO, Beyer MK, Sowa P, Nordvik JE, Kolskår K, Richard G, Andreassen OA, Harbo HF, Westlye LT, 2019. Cross-Sectional and Longitudinal MRI Brain Scans Reveal Accelerated Brain Aging in Multiple Sclerosis. Front Neurol 10, 450. 10.3389/fneur.2019.00450 [PubMed: 31114541]

Khalil M, Langkammer C, Pichler A, Pinter D, Gattringer T, Bachmaier G, Ropele S, Fuchs S, Enzinger C, Fazekas F, 2015. Dynamics of brain iron levels in multiple sclerosis: A longitudinal 3T MRI study. Neurology 84, 2396–2402. 10.1212/WNL.0000000000001679 [PubMed: 25979698]

Kruit MC, Launer LJ, Overbosch J, van Buchem MA, Ferrari MD, 2009. Iron accumulation in deep brain nuclei in migraine: A population-based Magnetic Resonance Imaging study. Cephalalgia 29, 351–359. 10.1111/j.1468-2982.2008.01723.x [PubMed: 19025553]

Kuhn DM, Ruskin B, Lovenberg W, 1980. Tryptophan hydroxylase. The role of oxygen, iron, and sulfhydryl groups as determinants of stability and catalytic activity. J Biol Chem 255, 4137–4143. [PubMed: 7372670]

Langkammer C, Schweser F, Krebs N, Deistung A, Goessler W, Scheurer E, Sommer K, Reishofer G, Yen K, Fazekas F, Ropele S, Reichenbach JR, 2012. Quantitative susceptibility mapping (QSM) as a means to measure brain iron? A post mortem validation study. NeuroImage 62, 1593–1599. 10.1016/j.neuroimage.2012.05.049 [PubMed: 22634862]

Lee MA, Blamire AM, Pendlebury S, Ho KH, Mills KR, Styles P, Palace J, Matthews PM, 2000. Axonal injury or loss in the internal capsule and motor impairment in multiple sclerosis. Arch Neurol 57, 65–70. 10.1001/archneur.57.1.65 [PubMed: 10634450]

Li J, Zhang Q, Che Y, Zhang N, Guo L, 2021. Iron Deposition Characteristics of Deep Gray Matter in Elderly Individuals in the Community Revealed by Quantitative Susceptibility Mapping and Multiple Factor Analysis. Frontiers in Aging Neuroscience 13, 166. 10.3389/fnagi.2021.611891

Li W, Wu B, Liu C, 2011. Quantitative susceptibility mapping of human brain reflects spatial variation in tissue composition. Neuroimage 55, 1645–1656. 10.1016/j.neuroimage.2010.11.088 [PubMed: 21224002]

Macías Islas MÁ, Ciampi E, 2019. Assessment and Impact of Cognitive Impairment in Multiple Sclerosis: An Overview. Biomedicines 7, E22. 10.3390/biomedicines7010022

Manoliu A, Riedl V, Doll A, Bäuml JG, Mühlau M, Schwerthöffer D, Scherr M, Zimmer C, Förstl H, Bäuml J, Wohlschläger AM, Koch K, Sorg C, 2013. Insular Dysfunction Reflects Altered Between-Network Connectivity and Severity of Negative Symptoms in Schizophrenia during Psychotic Remission. Front Hum Neurosci 7, 216. 10.3389/fnhum.2013.00216 [PubMed: 23730284]

McKeown MJ, Hansen LK, Sejnowsk TJ, 2003. Independent component analysis of functional MRI: what is signal and what is noise? Curr Opin Neurobiol 13, 620–629. 10.1016/j.conb.2003.09.012 [PubMed: 14630228]

Mori S, Oishi K, Jiang H, Jiang L, Li X, Akhter K, Hua K, Faria AV, Mahmood A, Woods R, Toga AW, Pike GB, Neto PR, Evans A, Zhang J, Huang H, Miller MI, van Zijl P, Mazziotta J, 2008. Stereotaxic white matter atlas based on diffusion tensor imaging in an ICBM template. Neuroimage 40, 570–582. 10.1016/j.neuroimage.2007.12.035 [PubMed: 18255316]

Najdenovska E, Alemán-Gómez Y, Battistella G, Descoteaux M, Hagmann P, Jacquemont S, Maeder P, Thiran J-P, Fornari E, Bach Cuadra M, 2018. In-vivo probabilistic atlas of human thalamic nuclei based on diffusion- weighted magnetic resonance imaging. Sci Data 5, 180270. 10.1038/sdata.2018.270 [PubMed: 30480664]

Pirpamer L, Hofer E, Gesierich B, De Guio F, Freudenberger P, Seiler S, Duering M, Jouvent E, Duchesnay E, Dichgans M, Ropele S, Schmidt R, 2016. Determinants of iron accumulation in the normal aging brain. Neurobiol Aging 43, 149–155. 10.1016/j.neurobiolaging.2016.04.002 [PubMed: 27255824]

Ramos P, Santos A, Pinto NR, Mendes R, Magalhães T, Almeida A, 2014. Iron levels in the human brain: a post-mortem study of anatomical region differences and age-related changes. J Trace Elem Med Biol 28, 13–17. 10.1016/j.jtemb.2013.08.001 [PubMed: 24075790]

Ravanfar P, Loi SM, Syeda WT, Van Rheenen TE, Bush AI, Desmond P, Cropley VL, Lane DJR, Opazo CM, Moffat BA, Velakoulis D, Pantelis C, 2021. Systematic Review: Quantitative Susceptibility Mapping (QSM) of Brain Iron Profile in Neurodegenerative Diseases. Front. Neurosci 15, 618435. 10.3389/fnins.2021.618435 [PubMed: 33679303]

Reichenbach JR, Schweser F, Serres B, Deistung A, 2015. Quantitative Susceptibility Mapping: Concepts and Applications. Clin Neuroradiol 25, 225–230. 10.1007/s00062-015-0432-9

Rissanen E, Tuisku J, Vahlberg T, Sucksdorff M, Paavilainen T, Parkkola R, Rokka J, Gerhard A, Hinz R, Talbot PS, Rinne JO, Airas L, 2018. Microglial activation, white matter tract damage, and disability in MS. Neurology - Neuroimmunology Neuroinflammation 5. 10.1212/NXI.0000000000000443

Salimi-Khorshidi G, Douaud G, Beckmann CF, Glasser MF, Griffanti L, Smith SM, 2014. Automatic Denoising of Functional MRI Data: Combining Independent Component Analysis and Hierarchical Fusion of Classifiers. Neuroimage 90, 449–468. 10.1016/j.neuroimage.2013.11.046 [PubMed: 24389422]

Schweser F, Deistung A, Lehr BW, Reichenbach JR, 2011. Quantitative imaging of intrinsic magnetic tissue properties using MRI signal phase: an approach to in vivo brain iron metabolism? Neuroimage 54, 2789–2807. 10.1016/j.neuroimage.2010.10.070 [PubMed: 21040794]

Schweser F, Deistung A, Reichenbach JR, 2016. Foundations of MRI phase imaging and processing for Quantitative Susceptibility Mapping (QSM). Z Med Phys 26, 6–34. 10.1016/j.zemedi.2015.10.002 [PubMed: 26702760]

Schweser F, Hagemeier J, Dwyer MG, Bergsland N, Hametner S, Weinstock-Guttman B, Zivadinov R, 2021. Decreasing brain iron in multiple sclerosis: The difference between concentration and content in iron MRI. Human Brain Mapping 42, 1463–1474. 10.1002/hbm.25306 [PubMed: 33378095]

Schweser F, Raffaini Duarte Martins AL, Hagemeier J, Lin F, Hanspach J, Weinstock-Guttman B, Hametner S, Bergsland N, Dwyer MG, Zivadinov R, 2018. Mapping of thalamic magnetic susceptibility in multiple sclerosis indicates decreasing iron with disease duration: A proposed mechanistic relationship between inflammation and oligodendrocyte vitality. Neuroimage 167, 438–452. 10.1016/j.neuroimage.2017.10.063 [PubMed: 29097315]

Schweser F, Sommer K, Deistung A, Reichenbach JR, 2012. Quantitative susceptibility mapping for investigating subtle susceptibility variations in the human brain. Neuroimage 62, 2083–2100. 10.1016/j.neuroimage.2012.05.067 [PubMed: 22659482]

Shin H-G, Lee Jingu, Yun YH, Yoo SH, Jang J, Oh S-H, Nam Y, Jung S, Kim S, Fukunaga M, Kim W, Choi HJ, Lee Jongho, 2021. χ-separation: Magnetic susceptibility source separation toward iron and myelin mapping in the brain. NeuroImage 240, 118371. 10.1016/j.neuroimage.2021.118371 [PubMed: 34242783]

Smith SM, Fox PT, Miller KL, Glahn DC, Fox PM, Mackay CE, Filippini N, Watkins KE, Toro R, Laird AR, Beckmann CF, 2009. Correspondence of the brain's functional architecture during activation and rest. PNAS 106, 13040–13045. 10.1073/pnas.0905267106 [PubMed: 19620724]

Snyder AM, Connor JR, 2009. Iron, the substantia nigra and related neurological disorders. Biochim Biophys Acta 1790, 606–614. 10.1016/j.bbagen.2008.08.005 [PubMed: 18778755]

Stankiewicz JM, Neema M, Ceccarelli A, 2014. Iron and multiple sclerosis. Neurobiology of Aging, International Conference on Nutrition and the Brain 35, S51–S58. 10.1016/j.neurobiolaging.2014.03.039

Stüber C, Pitt D, Wang Y, 2016. Iron in Multiple Sclerosis and Its Noninvasive Imaging with Quantitative Susceptibility Mapping. Int J Mol Sci 17, 100. 10.3390/ijms17010100 [PubMed: 26784172]

Tikhonov AN, Goncharsky A, Stepanov VV, Yagola AG, 1995. Numerical Methods for the Solution of Ill-Posed Problems. Springer Science & Business Media.

Walsh AJ, Lebel RM, Eissa A, Blevins G, Catz I, Lu J-Q, Resch L, Johnson ES, Emery DJ, Warren KG, Wilman AH, 2013. Multiple sclerosis: validation of MR imaging for quantification and detection of iron. Radiology 267, 531–542. 10.1148/radiol.12120863 [PubMed: 23297322]

Whitfield JB, Treloar S, Zhu G, Powell LW, Martin NG, 2003. Relative importance of female-specific and non-female-specific effects on variation in iron stores between women. Br J Haematol 120, 860–866. 10.1046/j.1365-2141.2003.04224.x [PubMed: 12614223]

Woo C-W, Krishnan A, Wager TD, 2014. Cluster-extent based thresholding in fMRI analyses: Pitfalls and recommendations. Neuroimage 91, 412–419. 10.1016/j.neuroimage.2013.12.058 [PubMed: 24412399]

Xu X, Wang Q, Zhang M, 2008. Age, gender, and hemispheric differences in iron deposition in the human brain: an in vivo MRI study. Neuroimage 40, 35–42. 10.1016/j.neuroimage.2007.11.017 [PubMed: 18180169]

Yim Y, Choi JD, Cho JH, Moon Y, Han S-H, Moon W-J, 2022. Magnetic susceptibility in the deep gray matter may be modulated by apolipoprotein E4 and age with regional predilections: a quantitative susceptibility mapping study. Neuroradiology. 10.1007/s00234-021-02859-9

Zivadinov R, Bergsland N, Cappellani R, Hagemeier J, Melia R, Carl E, Dwyer MG, Lincoff N, Weinstock-Guttman B, Ramanathan M, 2014. Retinal nerve fiber layer thickness and thalamus pathology in multiple sclerosis patients. Eur J Neurol 21, 1137–e61. 10.1111/ene.12449 [PubMed: 24779967]

Zivadinov R, Rudick RA, Masi RD, Nasuelli D, Ukmar M, Pozzi–Mucelli RS, Grop A, Cazzato G, Zorzon M, 2001. Effects of IV methylprednisolone on brain atrophy in relapsing-remitting MS. Neurology 57, 1239–1247. 10.1212/WNL.57.7.1239 [PubMed: 11591843]

Zivadinov R, Tavazzi E, Bergsland N, Hagemeier J, Lin F, Dwyer MG, Carl E, Kolb C, Hojnacki D, Ramasamy D, Durfee J, Weinstock-Guttman B, Schweser F, 2018. Brain Iron at Quantitative MRI Is Associated with Disability in Multiple Sclerosis. Radiology 289, 487–496. 10.1148/radiol.2018180136 [PubMed: 30015589]

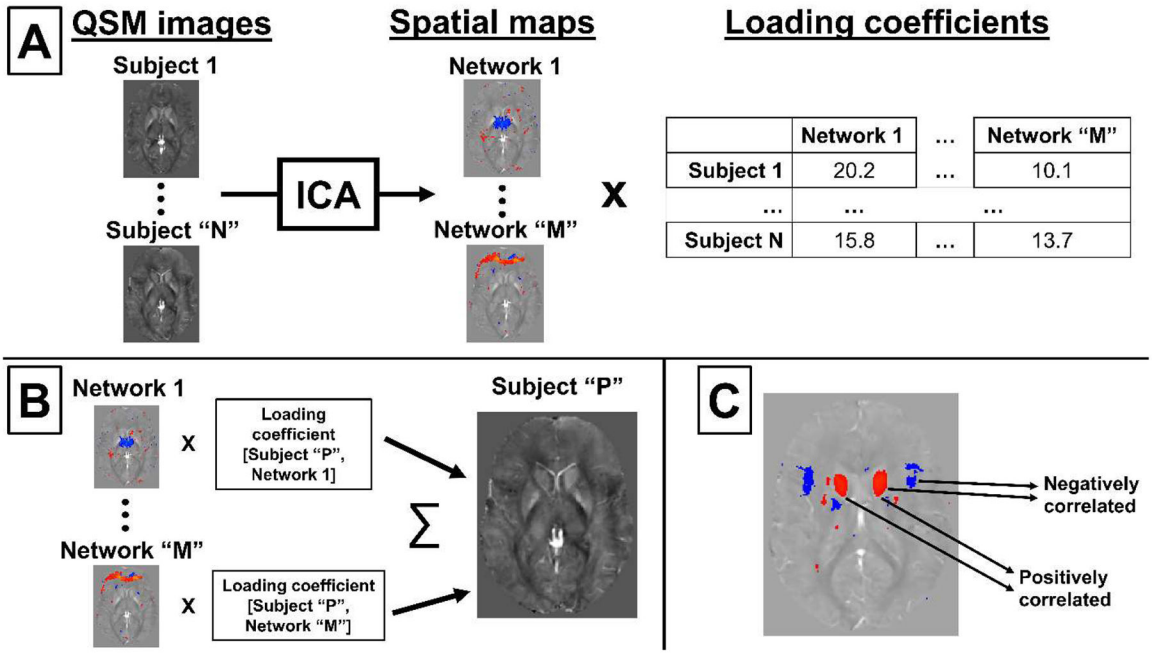

Figure 1. ICA methodology applied to QSM.

(A) Visual representation of the ICA network decomposition process. (B) Representation of the reconstruction of an original MRI scan from networks and loading coefficients. (C) Interpretation of ICA network spatial patterns.

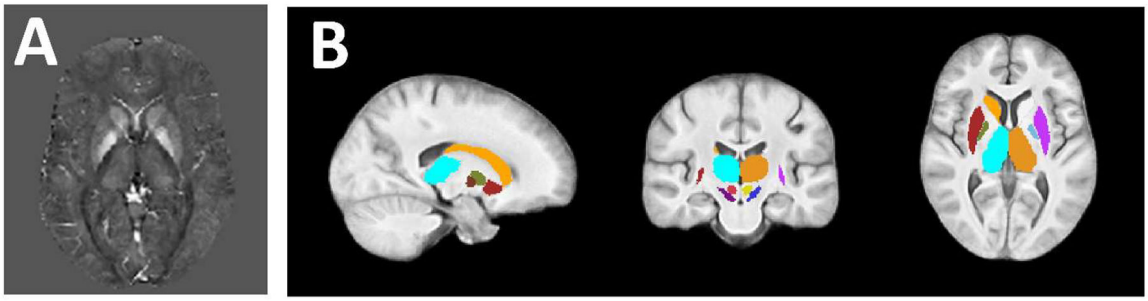

Figure 2. Sample susceptibility map and subcortical atlas.

(A) Representative template-normalized susceptibility map scaled from −0.1 ppm (black) to 0.2 ppm (white). (B) Subcortical atlas used to determine DGM-associated networks.

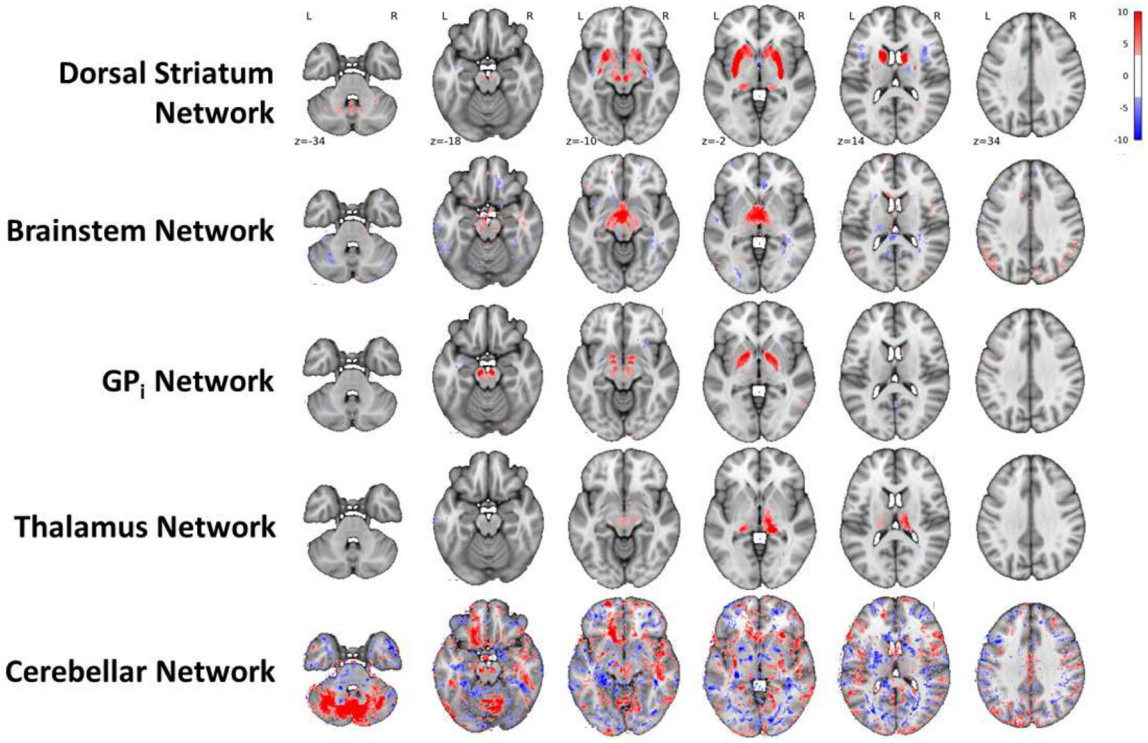

Figure 3. Five HA cohort networks.

Axial slices of the five HA cohort networks that were significantly associated with at least one DGM structure. Image threshold: $|Z| > 3.3$, corresponding to $P < 0.001$ two-tailed voxel-wise t tests uncorrected.

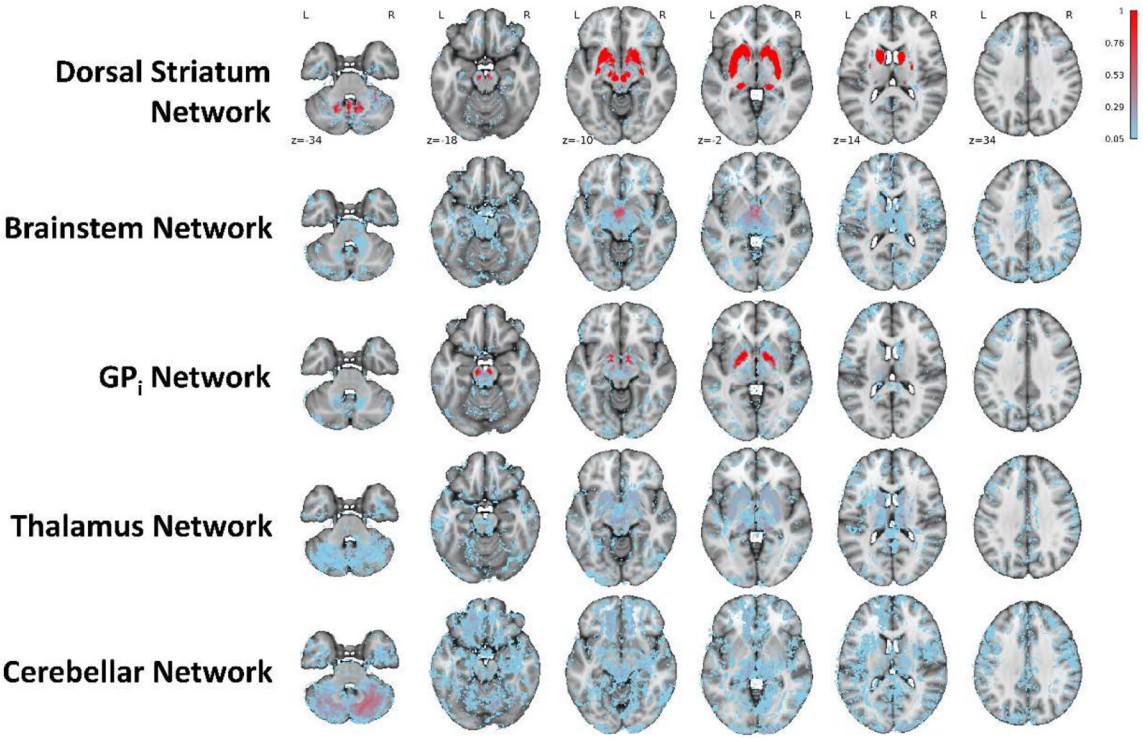

Figure 4. Robustness of HA Cohort Networks.

Probability maps showing the fraction of the 20 DGM network-matched ICA iterations that were significant ($|Z| > 3.3$) at each voxel. Transparent areas indicate voxels that were not significant for that network in any of the 20 iterations.

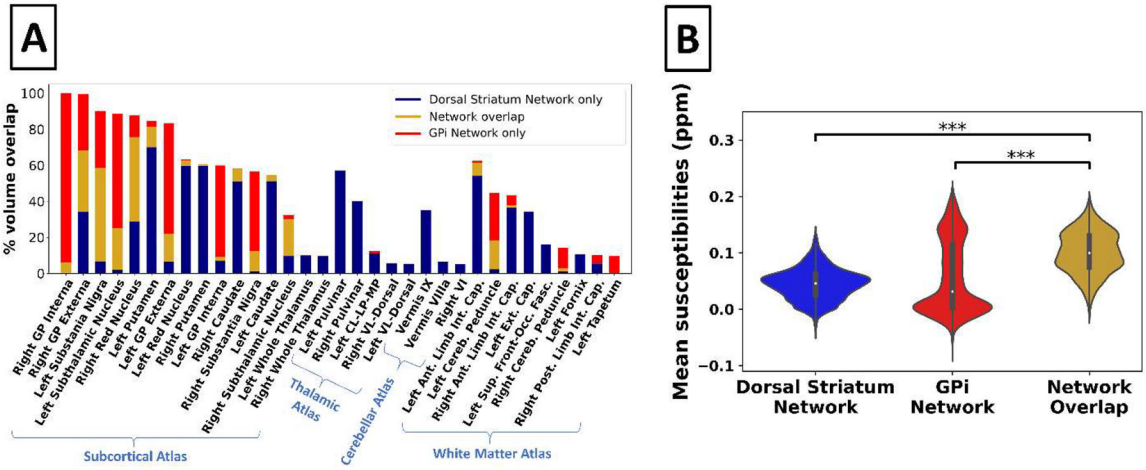

Figure 5. Anatomical overlap of the two robust HA cohort networks and susceptibility values in areas of network overlap.

(A) Bar graph showing the percent volume overlap of the robust DGM-associated networks within anatomical regions (threshold: $|Z| > 3.3$). Only DGM areas with > 5% overlap by volume are displayed. (B) Violin plots of susceptibility values of voxels in the subcortical atlas. ***$P < 0.0001$, Bonferroni corrected for two comparisons. Ant. = anterior; Cereb. = cerebellar; CL-LP-MP = central-lateral, lateral-posterior, and medial-pulvinar; Ext. Cap. = external capsule; Front-Occ. Fasc. = fronto-occipital fasciculus; GP = globus pallidus; Int. Cap. = internal capsule; Post. = posterior; Sup. = superior; VL = ventral-lateral.

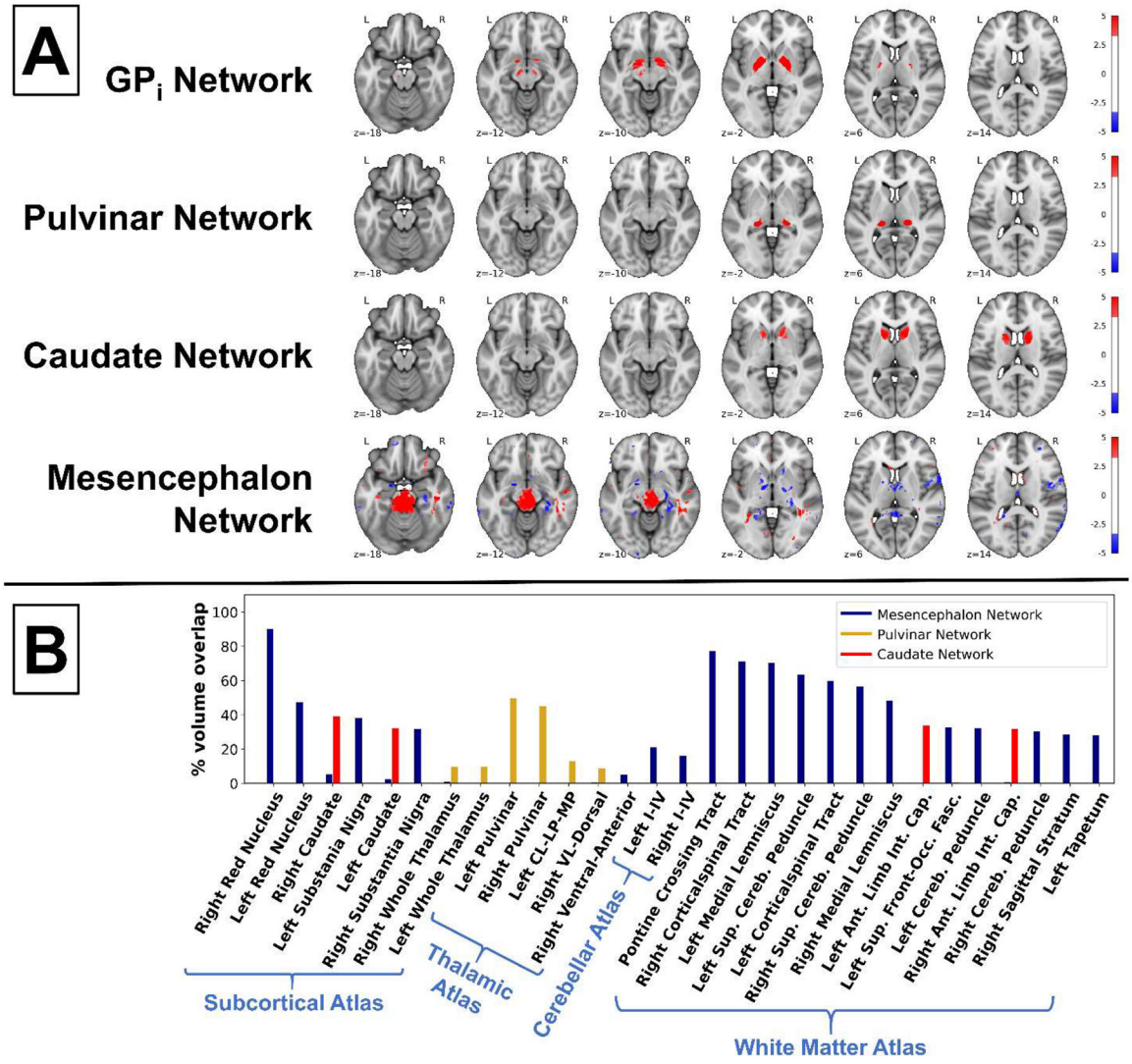

Figure 6. MS networks and their anatomical representations.

(A) Axial slices of the networks derived from the MS/HC cohort that had a significant main effect of disease status. Image threshold: $|Z| > 3.3$, corresponding to $P < 0.001$ two-tailed voxel-wise *t* tests, uncorrected. (B) Bar graph showing the percent volume overlap of additional disease-related MS/HC networks and anatomical regions (threshold: $|Z| > 3.3$). Only areas with > 5% overlap by volume are shown. Ant. = anterior; CL-LP-MP = central-lateral, lateral-posterior, and medial-pulvinar;

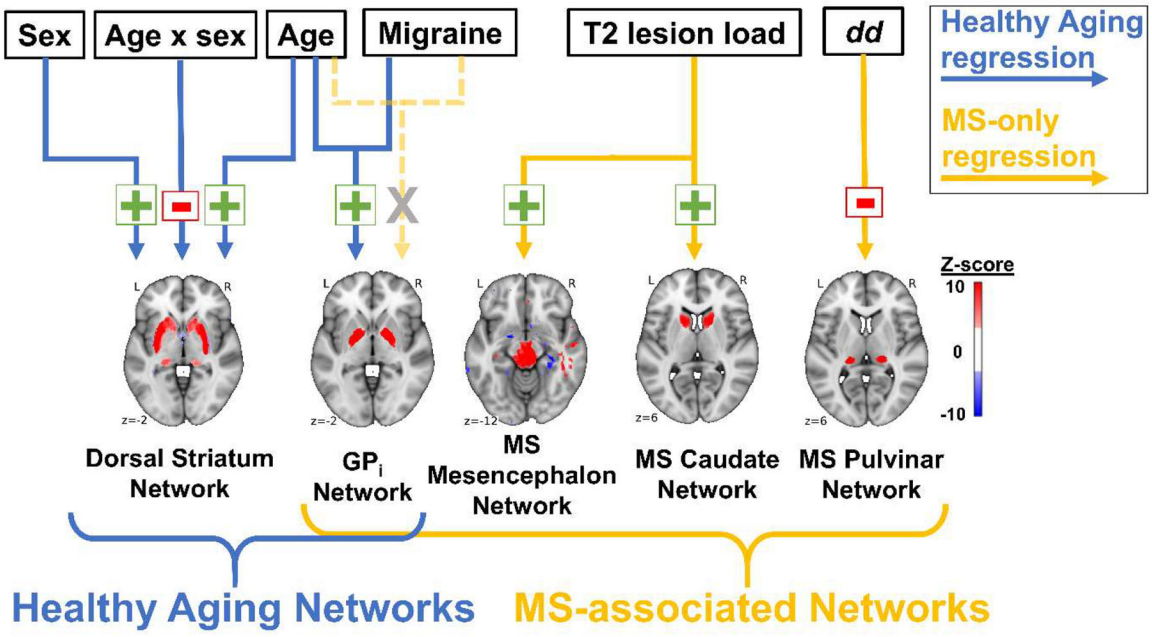

Figure 7. Diagram of the factors associated with the HA Networks and MS Networks.
Associations are shown separately for the HA cohort regression (blue arrows) and MS-only regression (gold arrows). Green plus sign = positive association; red negative sign = negative association; grey "X" = no association in MS cohort only.

Table 1

Cohort characteristics

Characteristic	HA cohort	MS/HC cohort							
		CIS	RRMS	SPMS	HC-CIS	HC-RRMS	HC-SPMS	All patients	All HC
Total cohort									
No.	170	40	40	40	40	40	40	120	120
Age, yrs (mean±SD [range])	39±17 (9–81)	37±10 (20–58)	44±10 (27–65)	52±7 (33–64)	37±12 (20–59)	43±10 (19–60)	53±12 (23–76)	44±11 (20–65)	45±13 (19–76)
Sex, no.									
Female	85	29	27	29	28	30	29	85	88
Male	85	11	13	11	12	10	11	35	33
dd, yrs (mean±SD)		2.2±2.6	9.8±6.0	24.0±10.2				12.1±11.3	
EDSS (median [range])		1.5 (0–4.5)	2.0 (0–8)	6.5 (2.5–8)				2.5 (0–8)	
ICA final cohort									
No.	166	40	40	38	39	37	39	118	115
Age, yrs (mean±SD [range])	39±16 (9–81)	37±10 (20–58)	44±10 (27–65)	52±7 (33–64)	37±12 (20–59)	43±10 (19–60)	52±12 (23–76)	44±11 (20–65)	44±13 (19–76)
Sex, no.									
Female	83	29	27	29	27	28	28	85	83
Male	83	11	13	9	12	9	11	33	32
dd, yrs (mean±SD)		2.2±2.6	9.8±6.0	24.1±10.1				11.7±11.3	
EDSS (median [range])		1.5 (0–4.5)	2.0 (0–8)	6.5 (2.5–8)				2.5 (0–8)	
Regression cohort									
No.	70	30	31	30	32	28	33	91	93
Age, yrs (mean±SD [range])	44±15 (12–76)	38±11 (20–58)	44±10 (27–65)	53±7 (33–64)	37±12 (20–59)	43±10 (19–60)	52±11 (26–76)	45±11 (20–65)	44±13 (19–76)
Sex, no.									
Female	39	23	19	22	22	18	25	64	65
Male	31	7	12	8	10	10	8	27	28
Systolic BP (mean±SD)	131±14	133±19	137±21	140±22	132±15	133±18	131±16	137±21	132±16
BMI (mean±SD)	27.0±5.9	26.4±6.1	26.8±6.3	25.5±4.3	25.4±5.4	28.7±5.8	26.5±5.4	26.2±5.6	26.8±5.6
Current smoker									
Yes	14	2	3	1	0	1	0	6	1
No	56	28	28	29	32	27	33	85	92
Reported migraines									
Yes	13	3	5	3	7	9	4	11	20
No	57	27	26	27	25	19	29	80	73
dd, yrs (mean±SD)		2.0±2.4	10.0±6.3	25.1±9.3				12.4±11.6	
EDSS (median [range])		1.5 (0–4.5)	2.5 (0–8)	6.1 (2.5–8)				3.3 (0–8)	

Table 2

Results of exploratory DGM network regression models

Variable	Network for HA cohort[a]		Network for MS-only cohort[a]			
	Dorsal striatum	**GP_i**	**GP_i**	**Pulvinar**	**Caudate**	**Mesencephalon**
Adjusted R^2	0.175	0.194	0.171	0.234	0.096	0.039
Age	**1.176 (0.004)** **	**0.377 (0.004)** **	0.098 (0.524)	−0.037 (0.795)	0.228 (0.146)	0.083 (0.588)
Sex	**0.811 (0.022)** *	−0.060 (0.598)	0.122 (0.239)	0.067 (0.497)	0.066 (0.552)	0.153 (0.175)
Age × Sex	**−1.162 (0.021)** *	n.s.	n.s.	n.s.	n.s	n.s.
Systolic BP	0.075 (0.511)	0.211 (0.085)	−0.003 (0.976)	−0.194 (0.079)	−0.117 (0.361)	−0.097 (0.478)
BMI	0.176 (0.115)	0.017 (0.886)	−0.129 (0.219)	0.028 (0.764)	0.031 (0.771)	0.021 (0.856)
Smoking	0.052 (0.651)	−0.212 (0.086)	0.197 (0.066)	−0.091 (0.369)	0.103 (0.371)	0.095 (0.410)
Migraine	0.061 (0.594)	**0.285 (0.022)** *	0.050 (0.645)	0.088 (0.391)	−0.090 (0.439)	0.100 (0.390)
dd	-	-	−0.003 (0.986)	**-0.488 (0.005)** **	0.076 (0.680)	0.291 (0.141)
T2 lesion volume	-	-	0.161 (0.131)	0.047 (0.643)	**0.272 (0.018)** *	**0.288 (0.013)** *
EDSS	-	-	0.306 (0.080)	0.106 (0.518)	0.113 (0.545)	0.361 (0.057)

[a] Standardized beta values are given with uncorrected P values below in parentheses. Significant effects are bolded. “n.s.” indicates a nonsignificant age × sex term that was removed from the final model.

* $P < 0.05$

** $P < 0.01$.

Table 3

Results of exploratory ROI-based regression models

Variable	Putamen	Pulvinar	Caudate
Adjusted R^2	0.150	0.016	0.037
Age	**0.514 (0.001)** **	−0.009 (0.958)	0.163 (0.314)
Sex	0.082 (0.444)	0.034 (0.772)	0.057 (0.618)
Age × Sex	n.s.	n.s.	n.s.
Systolic BP	−0.158 (0.192)	−0.154 (0.236)	−0.095 (0.462)
BMI	−0.059 (0.582)	0.142 (0.223)	0.047 (0.680)
Smoking	−0.159 (0.139)	**−0.244 (0.036)** *	−0.002 (0.989)
Migraine	0.045 (0.665)	−0.070 (0.535)	0.091 (0.413)
dd	−0.182 (0.331)	−0.183 (0.365)	0.234 (0.242)
T2 lesion volume	0.036 (0.757)	0.135 (0.365)	0.145 (0.244)
EDSS	0.150 (0.408)	0.081 (0.678)	−0.082 (0.672)

[a]Standardized beta values are given with uncorrected P values in parentheses. Significant effects are bolded. “n.s.” indicates a nonsignificant age × sex term that was removed from the final model.

*$P < 0.05$

**$P < 0.01$.